sciendo

POLISH MARITIME RESEARCH 2 (106) 2020 Vol. 27; pp. 11-18
10.2478/pomr-2020-0022

EXPERIMENTAL STUDY ON DYNAMIC STRUCTURE OF PROPELLER TIP VORTEX

Li Guangnian[1]
Qingren Chen[2]
Yue Liu[2]
[1] Ningbo University, China
[2] Wuhan Rules and Research Institute, China

ABSTRACT

Propeller cavitation is a main source of fluctuating pressure and noise induced by propellers, and the tip vortex cavitation is the principal source. The present study measures the flow fields near the blade tip using the 2D-PIV technique. The experimental setup and scheme are introduced. We monitor the process of generation and shedding of the propeller tip vortex in real time and analyse the dynamic structure of the tip vortex by testing the propeller wake field under different phases of the axial plane. The distribution characteristics of radial and axial velocity are also analysed. The influence range and the vorticity of the tip vortex and trailing vortex are obtained. All of the measured quantitative data are useful for future propeller design.

Keywords: propeller; blade tip; tip vortex; PIV

INTRODUCTION

With the recent trend in shipping towards large-scale and high-speed vessels, the application of high-power and heavy-load propellers is widely increasing. On the one hand, due to increased propeller load, easier propeller cavitation leads to many serious problems, including hull vibration and propeller noise. On the other hand, due to the higher requirements of tactics and technique indexes of the navigation and acoustic–stealth performance of warships and underwater weapons, the key issue is still a combination of the performance of propeller hydrodynamics, cavitation, and noise. [8] Thus, higher requirements are proposed for the design of the propeller. The evolution of the dynamic structure of the flow around propeller blades can affect hydrodynamics, radiated noise, and dynamic load of the propeller, which are the basis for the optimal design of propellers. Hence, it is significant to explore the generation, concentration, and shedding of free vortex and the micro-dynamic structure of flow around the propeller blades. In recent years, a lot of research on micro-dynamic structure and the propeller wake model have been carried out.

According to the propeller lifting line theory, free vortexes are formed by the cross flow around the blade tips. Free vortex shedding from the trailing edge is concentrated. A vortex flow rushes from the blade tip to the rear of the propeller. Due to the propeller rotation, the free vorticity at the tip is shed downstream as a spiral vortex line. [7] The propeller is usually installed at the rear of the hull. At the front of the propeller, the non-symmetrical hull, the various appendages, the propeller shaft, and the bracket cause uneven spatial and temporal distribution of flow on the propeller disk surface. These aggravate the complexity of the analysis of propeller turbulent flow.

Traditional methods for propeller performance analysis – such as the lifting line method, lifting surface method, and boundary element method – are based on potential flow theory, but they have some limitations around capturing flow field details [5] [11]. In recent years, the CFD method based on viscous flow theory has shown its superiority [2] [6] [19]. Liu et al. [4] simulated the cavitation of a rear propeller using the RANS solver combined with the SST k-ω turbulence model and Sauer cavitation model. Compared with test results in

a large circulating water channel, the dynamic behaviour of the propeller cavitation with spatial angle was in good agreement, although the blade tip vortex cavitation could not be captured due to the coarse grids. Pu et al. [10] employed a detached eddy simulation (DES) to simulate tip vortex in the propeller wake. In order to study the spatial shape of the propeller tip vortex, the 'Q criterion' of vortex core identification was used to define the isosurface of the propeller tip vortex. The results show that the numerical method can accurately predict the vortex distribution of the propeller wake field and the shape of the vortex core, which is in agreement with the experimental results. Although the CFD method has great advantages in the analysis of the microscopic flow field, the accuracy of CFD still needs experimental verification, and the model test of the propeller cannot be replaced completely [1] [16] [17].

Due to the characteristics of the high frequency pulsation of the propeller wake, it is difficult to measure the flow field of the propeller using traditional measuring instruments such as a pitot tube and hot wire anemometer. The development of laser Doppler velocimeter (LDV) and particle image velocimetry (PIV) technology has resulted in more advanced tools for measuring the flow field of rotating machines, such as propellers. The earliest application of LDV to the measurement of propeller flow field was by Min [12], who first used LDV to explore the microstructure of flow field around the propeller. Later, the LDV method matured to better measure propeller flow, making a significant contribution to the experimental study of the progress of wake flow and the flow structure of the blade tip. Jessup et al. [9] and Dong et al. [18] used LDV to measure the flow field of propeller wake in detail. Jessup analysed vortex distribution based on the velocity field obtained by LDV for a DTRC 4119 propeller. Shown in Fig. 1a, the magnitude of space occupied by the tip vortex can be observed. However, the vortex contour does not start from zero, so the distribution range of the tip vortex should be larger than that shown in Fig. 1a. The region of the tip vortex and trailing flow analysed based on velocity loss are shown in Fig. 1b, which shows the region of the tip vortex, ranging from 0.93R to 0.99R.

Compared with single-point LDV, PIV has a greater advantage for instantaneous and full-field measurement. Thus, it is good at measuring the complex structure of wake flow field around the propeller. Cotrooni [3] and Lee [14] have used PIV to measure the propeller wake field successfully. Paik et al. [15] used PIV to study the effects of a free surface on the wake behind a rotating propeller at a rather low Reynolds number. Lee et al. [13] employed PIV to investigate the flow characteristics of the hull wake behind a container ship model under different loading conditions. Most of the previous works using PIV pay attention to the evolution of the tip vortex in the wake. Results show that the tip vortex is a Rankine vortex, which forms a spiral vortex line behind the propeller, moves down along the trailing flow, and contracts steadily. The pitch angle of the tip vortex line increases gradually until the tip vortex line oscillates and disappears far downstream. These results have improved the Kelvin vortex model. However, there is little research on the evolutionary process – from free vortex concentration, to the formation of the tip vortex, to vortex shedding – which play an important role in the improvement of numerical models based on propeller circulation theory.

The present paper uses the advanced PIV system to study the characteristics of tip flow field of a DTMB-P4119 propeller in a large cavitation tunnel, focusing on the process of the concentration of free vortex into the formation and shedding of the tip vortex, the structure of the tip vortex, and the evolution of the tip vortex in the wake of flow fields. We hope that the present work can give insights into the design and optimization of propellers.

EXPERIMENTAL SETUP

The large cavitation tunnel of the China Ship Scientific Research Center has a test section length of 3.2 m and diameter of 0.8 m. The flow speed range is from 3 to 20 m/s. We chose the DTMB-P4119 propeller as the test object, which is a right-handed propeller with three blades and hub diameter ratio of 0.2. The propeller does not skew or rake. The design load of the propeller is $J = 0.833$ and the diameter is 250 mm. The experiments were carried out under two test conditions, as shown in Table 1. The dynamometer installed on the shaft has a maximum rotational speed of 4500 rpm, a maximum range of thrust of 4000 N, a maximum range of torque of 500 N.m, and a minimum cavitation number of 0.5. The control parameters of this experiment are velocity and pressure of water, and rotational speed of propeller. The velocity of water and pressure are measured by the differential pressure transmitter through the test holes. The rotational

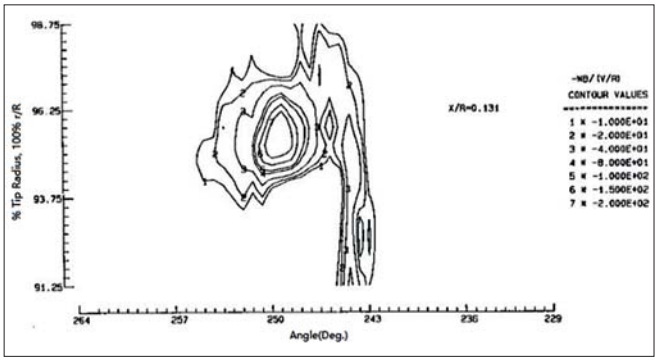

Fig. 1a. Vortex strength distribution of DTRC 4119 tip vortex

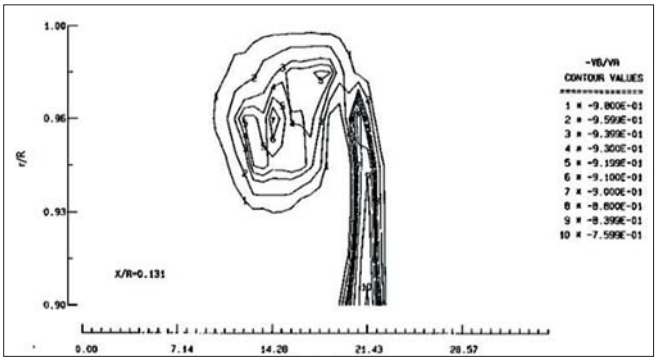

Fig. 1b. Velocity contour curves of the trailing vortex and tip vortex

speed is measured by a 1024-line grating encoder mounted on the shaft. The control accuracy of velocity and pressure is 0.5% and the rotational speed is 0.1%.

Table 1. Test Conditions

	water velocity (m/s)	rotational speed of propeller (rps)	advance ratio *J*
1	3.544	23.67	0.600
2	3.544	17.06	0.833

A BigSky-190 pulse laser with a maximum pulse energy of 325 mJ/pulse and a maximum pulse repetition rate of 10 Hz was chosen. We adapted the laser to make sheet lighting from the side windows of the tunnel. The sheet-light spread along the horizontal axis of the tunnel, with a thickness of 1.5 mm. A TSI PowerView 4M camera with a resolution of 2048*2048 pixels was used to take pictures from the observation window on the bottom surface of the tunnel. The test surface for taking pictures was 110 mm*110 mm, as shown in Fig. 2. Pine pollen were the chosen tracing particles, with a diameter of about 40 μm and a density of 0.95 g/cm^3. In the test, an equal phase signal sent by the processor of a shaft encoder was received by the synchronous controller, which was delayed to control the laser and camera. Each experiment group only took photos of the particles in the same phase. We set the direction of the flow as a positive *X* axis and vertical direction through the centre of the propeller disk as the positive *Z* axis. The *Y* axis was determined by the right-hand rule. The test area of *z/R* ranged from 0.37 to 1.23, and *x/R* from 0.28 to 0.57. As shown in Fig. 3, the propeller reference line was regarded as the zero degree of the moving coordinate system. The horizontal meridian plane was considered to be the zero degree of the stationary coordinate system. The rotation direction of the propeller was defined as the positive direction. The axial and radial velocity field of the propeller wake field within phase from 0° to 120° were measured every 5 degrees. The interval was more intensive in some regimes. The image analysis of PIV uses INSIGHT 3G software developed by the TSI company. The size of the diagnostic window was 42*42 pixels and the imaging coefficient was 0.053; hence, the real size was about 2.2 mm*2.2 mm.

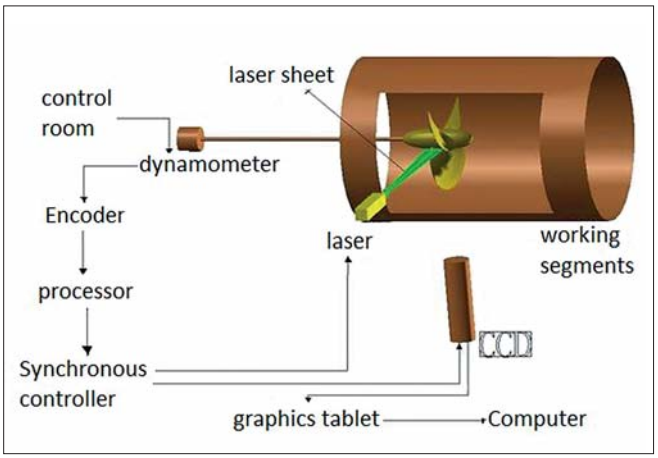

Fig. 2. Measurement planes

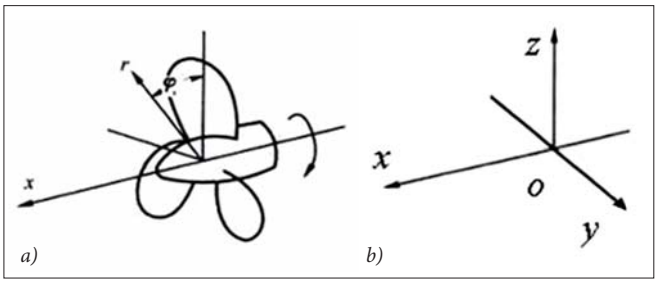

Fig. 3. Schematics of PIV measurements for the propeller

The present work uses a two-dimensional testing technology to measure three-dimensional motion; hence, there is an error. The error may originate from the PIV system, such as the laser, tracing particle, delay generator, or the camera. The light sheet emitted by the laser should be thin enough and the concentration of tracing particles in the measurement domain should reach a certain level to extract correct velocity vectors. To reduce the measurement uncertainty with respect to the two factors to an acceptable level, a sheet-light thickness of 1.5 mm and a particle diameter of about 40 μm were chosen. According to the principle of PIV measurement, a cross-section velocity field was obtained which required two camera exposures. The exposure time interval in test was set to 100 μs and, during the exposure period, the average displacement of particles in the two adjacent particle images was about 4–5 pixels. Taking the propeller speed as 23.67 rps, the propeller blades rotated 0.85° in the time interval of 100 μs, so that the phase resolution of the test was high enough compared with the angular spacing of 120° between two adjacent blades. Other measurement errors, such as propeller speed and incoming flow velocity, affected the test results. In order to minimize measurement uncertainty, the value of the velocity field at the same phase was the average of the experimental data from 100 measurements.

ANALYSIS OF DATA

Before PIV measurement for flow fields in test conditions of *J* = 0.6, 0.833, the thrust of the propeller in the cavitation tunnel was measured at the advance ratio *J* = 0.6-1.09. Fig. 4

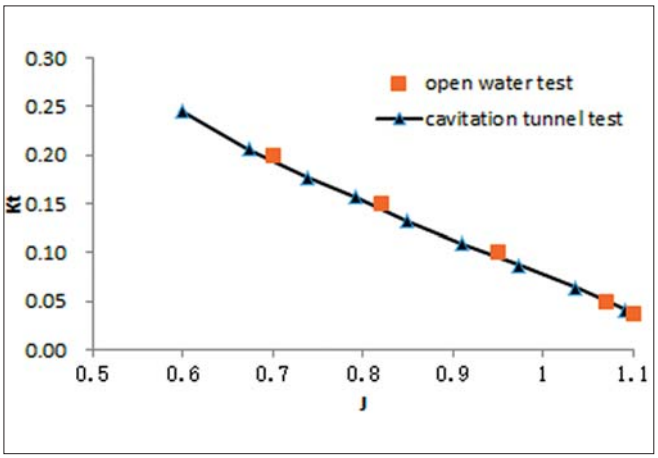

Fig. 4. Comparisons of thrust coefficient

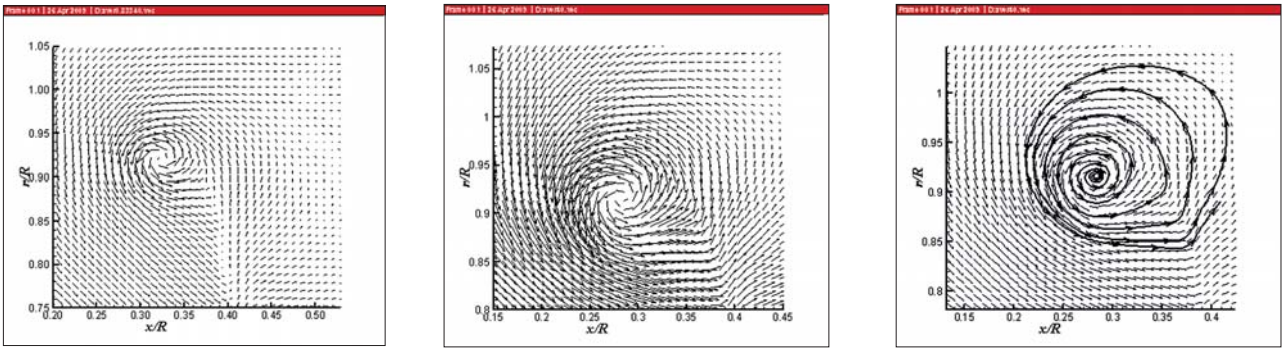

a) J = 0.833, φ = 40° *b) J = 0.6, φ = 40°* *c) Enlargement of b*

Fig. 5. Vector of tip vortex

shows the comparisons of thrust coefficient between present results and the open water test results [11] .These results reveal that the propeller thrusts in the cavitation tunnel test were a bit smaller than in open water when J<1.0.

In the flow field, U is the incoming flow velocity, u the axial velocity, v the radial velocity, and ω the vorticity. For all the results shown, the values of horizontal and vertical coordinates are the non-dimensional results by the radius of the propeller. Fig. 5 is the vector plot of the tip vortex flow field based on the experimental data. It can be seen that there is a clear spiral flow around the tip vortex, and the fluid is rolled-up into the tip vortex. We can also clearly observe from Fig. 5 that the propeller load is heavier, the tip vortex vector graphic becomes clearer, and the induced velocity is larger.

Fig. 6 shows distribution of the axial and radial velocities at the phase angles defined in Fig. 3 from $\varphi = 90°$ to $\varphi = 110°$ of the cross-section $x/R = 0.55$, in which a tip vortex is captured at a phase plane of about 100°. In the range for the radius between $r/R = 0.4$ and $r/R = 0.75$, there is a negligible difference between the velocities of every phase. However, for $0.75 < r/R < 1.0$, the axial and radial velocities of each phase are apparently different. The axial velocity of each phase at the tip vortex reduces sharply due to the loss of the axial velocity. The distribution of radial velocity near the tip vortex is related to the rotational direction of the vortex along the circumferential direction. Farther away from the vortex core, the mutation of induced radial velocity is much larger. When r/R>1.0, the velocity distribution for each phase gradually tends to relax. The loss of axial velocity slowly disappears. Axial velocity increases gradually to that of the incoming flow velocity, and the radial velocity decreases slowly to zero.

Fig. 7 shows the axial and radial velocity curves against the phase angle for the various radii of the cross-section at $x/R = 0.343$, which are close to the tip. The velocity jumps sharply on the circumference of the radii of $r/R = 0.833$, 0.851, and 0.869 during a rotation period of the propeller, caused by the test surface which passes through the trailing vortex. Comparing the axial and radial velocity curves of $r/R = 0.833$ and $r/R = 0.941$, there are two velocity jumps on the circumference during a rotation period; one is upward and the other is downward. At $r/R = 0.851$, the second upward protrusion begins to appear, and the protrusion becomes larger as the radius increases. After $r/R = 0.905$, the second protrusion quickly turns downward. With the increase of radius, the first protrusion becomes smaller and smaller until $r/R = 0.941$, where the first protrusion disappears. The tip vortex does not overlap with the trailing vortex sheet shedding from the blade. The measured surface passes through the trailing vortex sheet and the tip vortex successively, so there are two velocity jumps in the measurement, which is the cause of the occurrence of the two protrusions of velocity curves. [1] Based on above discussion, the influence range of the tip vortex can be roughly estimated by the distribution of double protrusions, of which the diameter is about $d = |r_{0.932} - r_{0.0.869}| = 0.063R$.

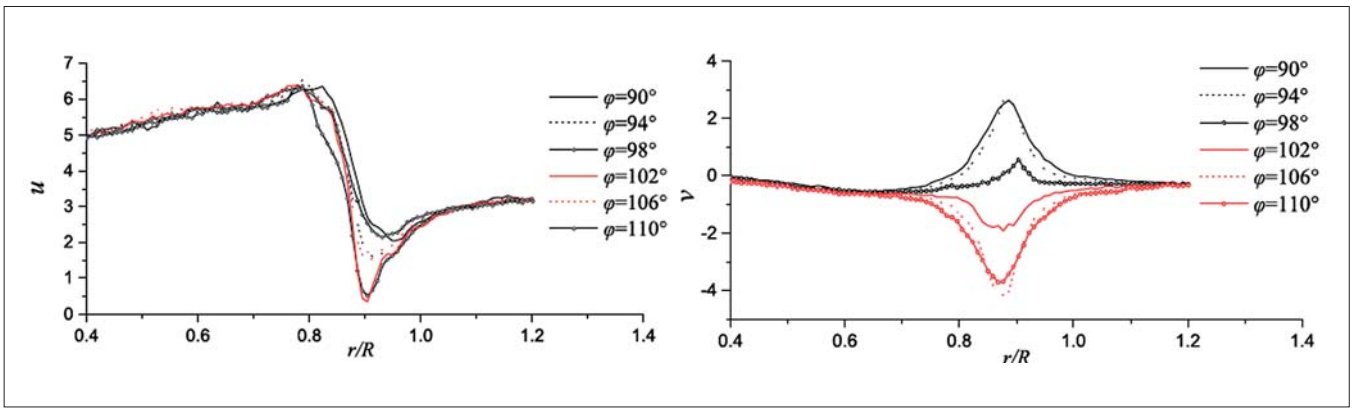

Fig. 6. Variation of axial and radial velocities at different phases at the cross-section of x/R = 0.55

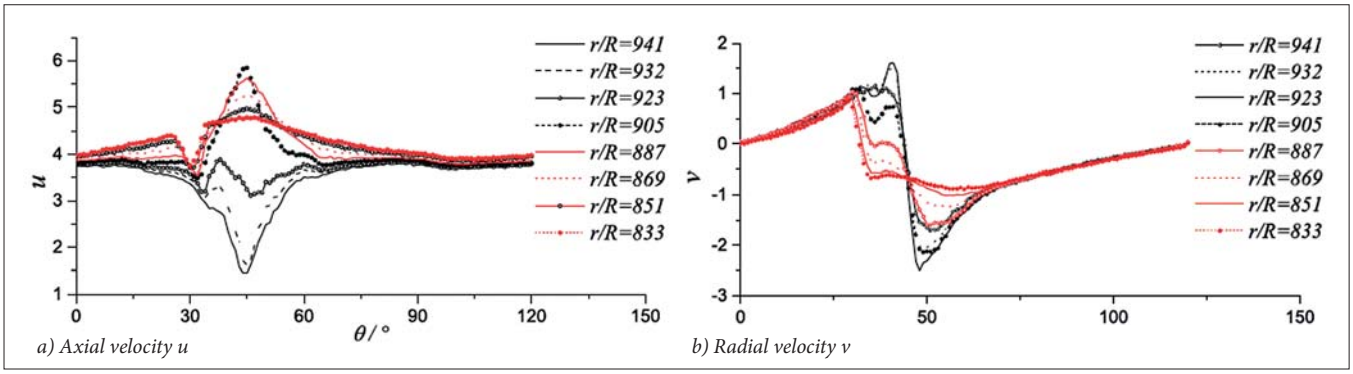

Fig. 7. Velocity at different radii in cross-section of x/R = 0.343

In the experiment, we only measured the axial and radial velocities of the propeller wake field, and the vorticity component in the Z direction can be calculated as follows:

$$\omega_2 = \frac{\partial v}{\partial x} - \frac{\partial u}{\partial y} \quad (1)$$

Fig. 8 shows the computed contour of vorticity. Fig. 9 presents the vorticity contour of the tip vortex. Fig. 10 shows part of the trailing vortex sheet. It can be seen from Figs. 8 and 9 that the vorticity of a trailing vortex increases with propeller load. At J = 0.833, the vorticity of the tip vortex core is 230, and at J = 0.6 increases to 270. The trailing vortex shedding form of the propeller trailing edge is obviously composed of two layers. This is primarily due to the existence of the boundary layer on the blade. The free vortex is separated into two layers with opposite directions. The positive vorticity extends from the blade tip to the propeller shaft along the trailing vortex sheet, and the intensity decreases gradually. The negative vorticity extends upward from the propeller shaft along the trailing vortex sheet, and the intensity decreases gradually too. At a certain radius, the vorticity values of both the positive and negative layers are equal (as shown in Fig. 9), and the rate change ($\Delta\Gamma \cdot \Delta r^{-1}$) of the circulation along radial direction is at a minimum. It is in agreement with the radial distribution of the circulation in design theory. With changes in circulation, the free vortex discharges and forms a spiral trailing vortex surface. The discharged free vortex intensity is $\Gamma_{FREE\_VORTEX} = \frac{\partial \Gamma_{BOUND\_VORTICITY}}{\partial r}$ dr. Closer to the outer radius, there is a larger rate of change in the circulation along the radial direction and a greater intensity of the discharged free vortex. At the tip of the blade, the free vortex intensity reaches a maximum and tip vortex shedding occurs. Fig. 11 shows the process clearly. At phase φ = 70° and blade trailing edge r/R = 0.82, it can be clearly seen that a positive free vortex cluster begins to gather. It can also be observed that the free vortex slowly climbs along the blade and the intensity increases gradually. At phase φ = 120° and blade trailing edge r/R=0.97, the free vortex drops off along the blade edge and forms the tip vortex. Repeating again and again, the continuous shedding of the tip vortex forms a spiral line. Fig. 12 shows the distribution of the radial coordinate of a vortex line in the flow wake. As shown in Fig. 12, data points of the tip vortex between $-0.1 < x/R < 0.1$ are a little discrete in the shedding process. This means that the tip vortex fluctuates violently during the process.

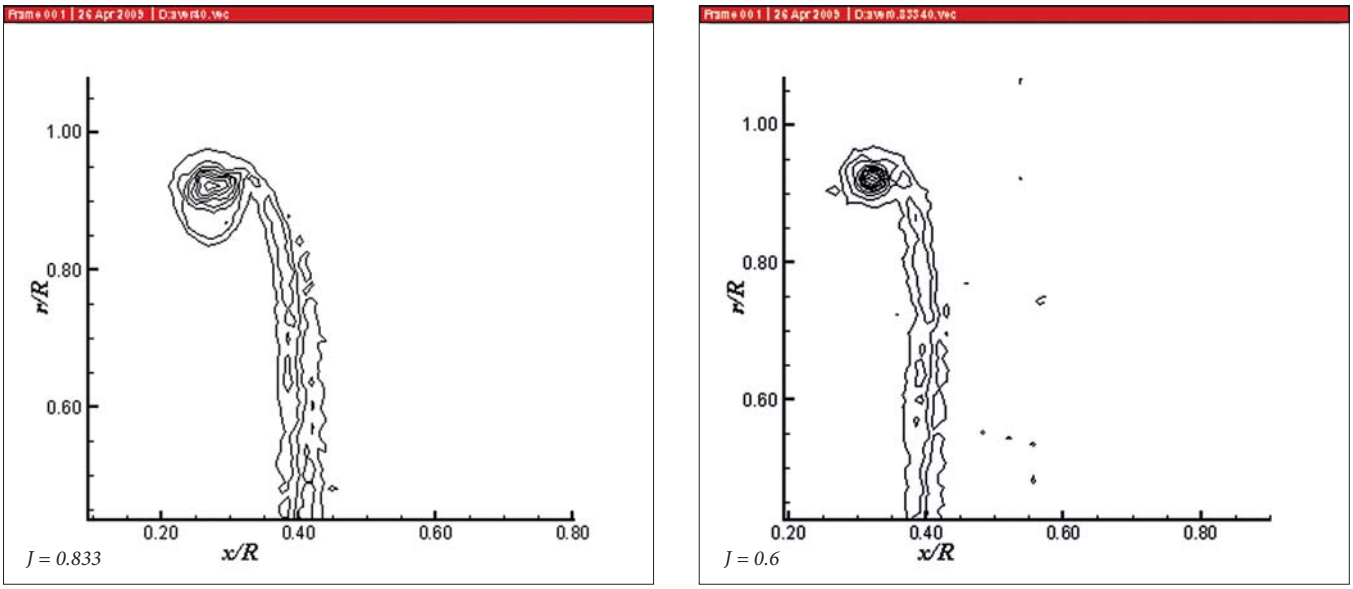

Fig. 8. Computed contour of vorticity which shows the trailing vortex

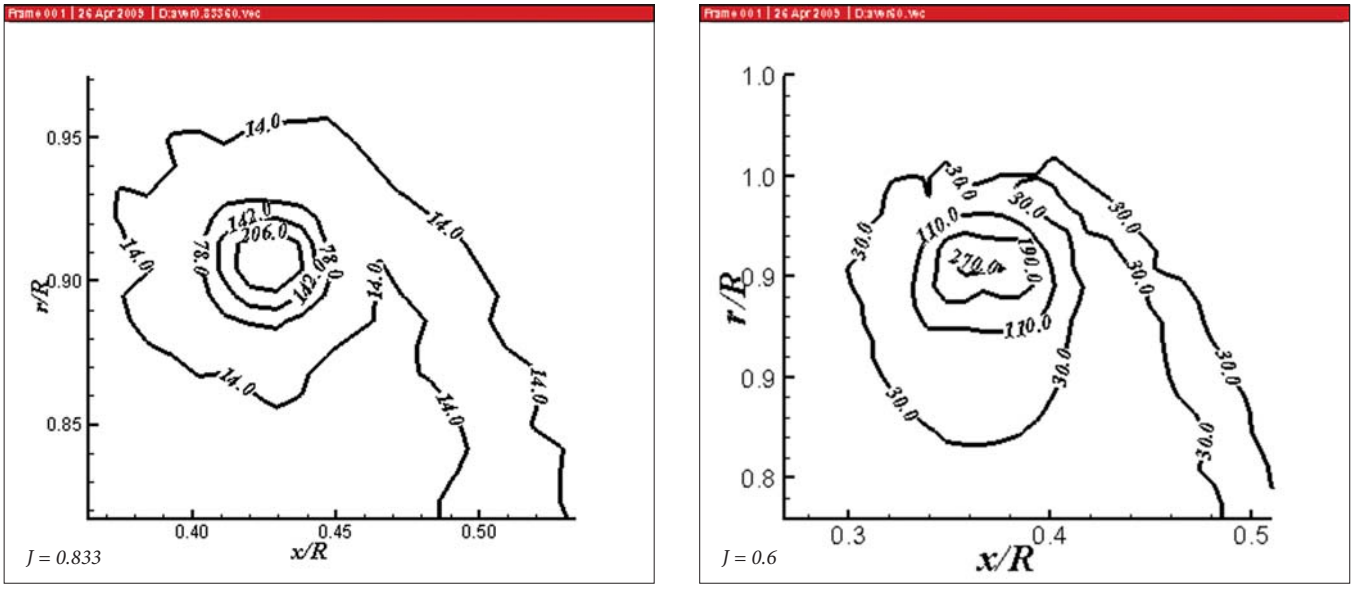

Fig. 9. Tip vortex φ = 60°

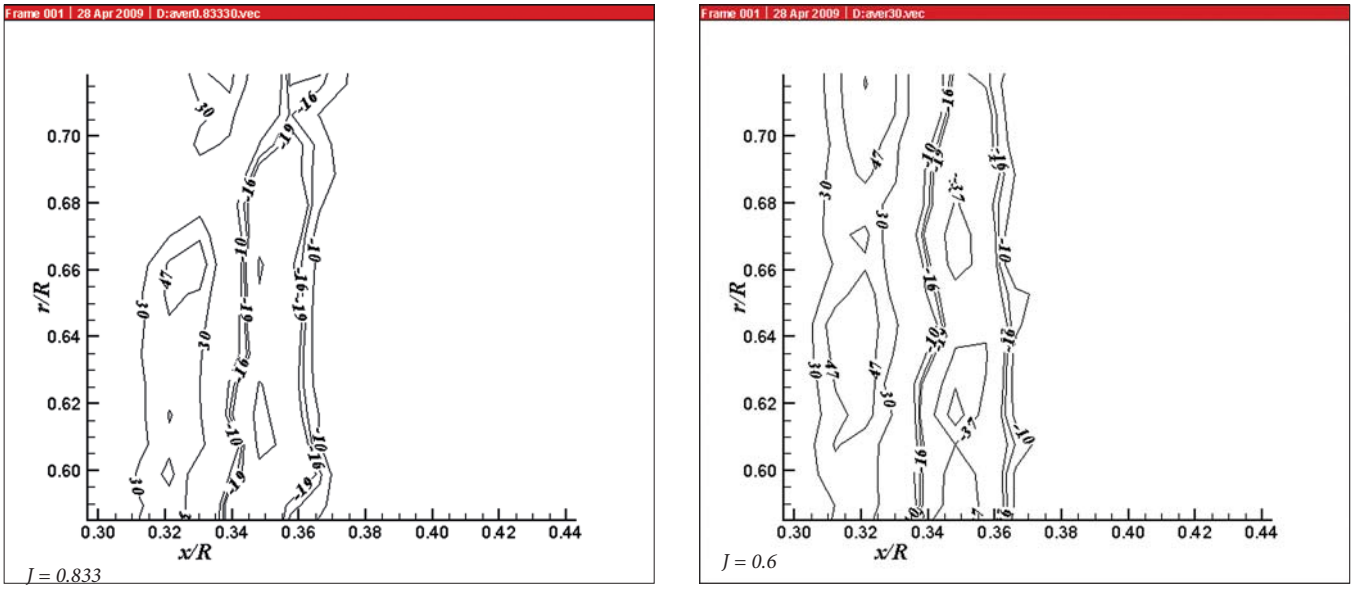

Fig. 10. Trailing vortex φ = 30°

CONCLUSION

Detailed measurements of the flow structure and shedding process of a propeller tip vortex in a cavitation tunnel were carried out in the present work and substantial flow field information was obtained. Although the analysis of the vorticity in the test area was only based on the axial and radial velocity fields, a number of characteristics of the flow field were obtained. The present study shows that the tip vortex sheds at blade trailing edge 0.97R. The influential range of a tip vortex in the wake is a sphere with a diameter of about 0.06R. The trailing vortex sheet is composed of two layers (positive and negative vorticity). Under the design load, the absolute vorticity of the positive and negative layers near 0.7R is equal. The quantitative data obtained from these experiments are useful for future propeller design.

This study was funded by the China National Natural Science Foundation Program (grant number 51679216), the project in Science and Technique Plans of Ningbo City Grant No. 2019C10091, the Natural Science Foundation of the Jiangsu Higher Education Institutions of China (Grant No. 18KJB580004), and sponsored by the K.C. Wong Magna Fund in Ningbo University.

REFERENCES

1. Aktas, B., Atlar, M., Turkmen, S., et al. (2016) *Systematic cavitation tunnel tests of a propeller in uniform and inclined flow conditions as part of a round robin test campaign*. Ocean Engineering, Vol. 120, 136–151.

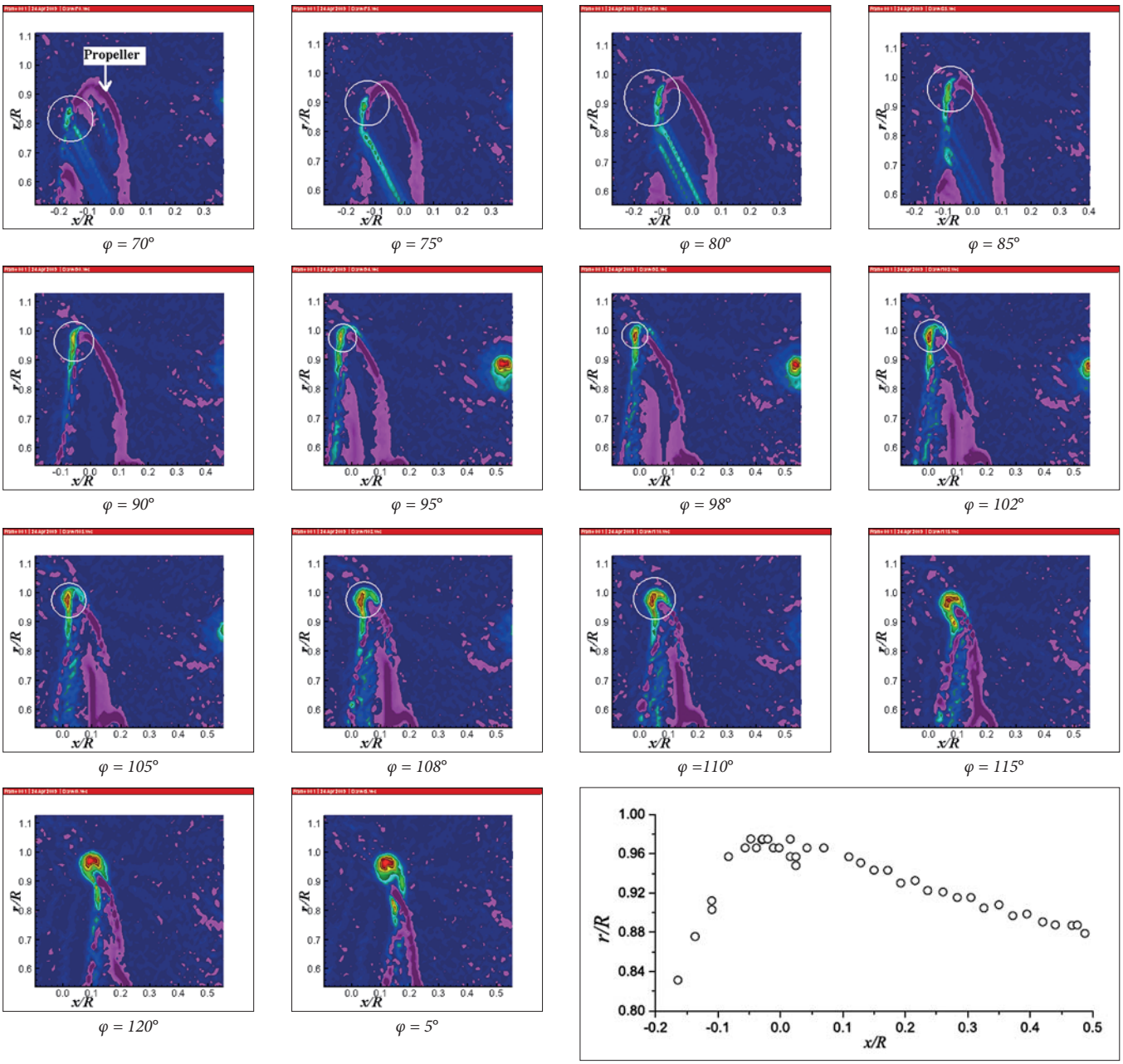

Fig. 11. Vorticity distribution of blade tip (J = 0.6)

Fig. 12. Trajectories of tip vortices J = 0.6

2. Baek, D.-G., Yoon, H.-S., Jung, J.-H., et al. (2015) *Effect of the advance ratio on the evolution of propeller wake*. Computers & Fluids, Vol. 118, 32–43.

3. Cotroni A., Felice F. D., Romano G. P., et al. (2000) *Investigation of the near wake of a propeller using particle image velocimetry*. Experiments in Fluids, Vol. 2000 (suppl), S227–S236.

4. Dengcheng, L., Weixin, Z. (2016) *Numerical predictions of the propeller cavitation behind ship and comparison with experiment*. Journal of Ship Mechanics. Vol. 20, No. 3, 233–242.

5. Gaggero, S., Gonzalez-Adalid, J., Perez-Sobrino, M. (2016) *Design of contracted and tip loaded propellers by using boundary element methods and optimization algorithms*. Applied Ocean Research. Vol. 55, 102–129.

6. Gaggero, S., Tani, G., Viviani, M., et al. (2014) *A study on the numerical prediction of propellers cavitating tip vortex*. Ocean Engineering, Vol. 92, 137–161.

7. Guoqiang, W., Shitang, D. (2005) *Theory and applications of marine propeller*. Harbin Engineering University Press, Vol. 5.

8. Guoqiang, W., Xiaolong, L. (2006) *Prediction of unsteady performance of ducted propellers by potential based panel method*. Journal of Ship Mechanics, Vol. 10, No. 1, 47–51.

9. Jessup, S. D. (1989) *An experimental investigation of viscous aspects of propeller blade flow*. Ph. D. Thesis, The Catholic University of America.

10. Jijun, P., Ying, X. *Scaling effects of propeller sheet cavitation*. Journal of Wuhan University of Technology, Vol. 40, No. 4, 705–708.

11. Koyama K. (1993) *Comparative calculations of propellers by surface panel method*. Workshop Organized by 20th ITTC Propulsor Committee, Ship Research Institute, Supplement, 15.

12. Min, K. S. (1978) *Numerical and experimental methods for prediction of field point velocities around propeller blades*. MIT Department of Ocean Engineering Report, Vol. 6.

13. Lee, J.-Y., Paik, B.-G., Lee, S. J. (2009) *PIV measurements of hull wake behind a container ship model with varying loading condition.* Ocean Engineering, Vol. 36, 377–385.

14. Lee S. J., Paik, B.-G., Yoon, J. H., et al. (2004) *Three-component velocity field measurements of propeller wake using a stereoscopic PIV technique*. Experiments in Fluids, Vol. 36, 575–585.

15. Paik, B.-G., Lee, C. M., Lee S. J. (2005) *Comparative measurement on flow structure of marine propeller wake between open free surface and closed surface flows*. Journal of Marine Science and Technology, Vol. 10(3), 123–130.

16. Pennings P. C., Westerweel J., Van Terwisga T. J. C. (2016) *Cavitation tunnel analysis of radiated sound from the resonance of a propeller tip vortex cavity*. International Journal of Multiphase Flow, Vol. 83, 1–11.

17. Tani, G., Villa, D., Gaggero, S., et al. (2017) *Experimental investigation of pressure pulses and radiated noise for two alternative designs of the propeller of a high-speed craft*. Ocean Engineering, Vol. 132, 45–69.

18. Zhengqing, D., Linzhang, L., Weixin, Z. (2006) *LDV measurements of inner velocity field of ducted propeller*. Journal of Ship Mechanics, Vol. 10, No. 5, 24–31.

19. Zhihui, L., Benlong, W., Xiaoxing, P. et al. (2016) *Calculation of tip vortex cavitation flows around three-dimensional hydrofoils and propellers using a nonlinear-kε turbulence model*. Journal of Hydrodynamics, Vol. 28, 227–237.

CONTACT WITH THE AUTHORS

Li Guangnian
e-mail: liguangnian@nbu.edu.cn
Ningbo University
Jiangbei, 316000 Ningbo
China

Qingren Chen
e-mail: cqr4891@126.com
Wuhan Rules and Research Institute
Aokou, 430070 Wuhan
China

Yue Liu
e-mail: yue.liu@unipd.it
Wuhan Rules and Research Institute
Aokou, 430070 Wuha2
China